引用格式：YANG Fulong, GUO Zhitao, FENG Zhe, et al. Double-layered Metasurface-based Dual-function Sensor for Detecting Ionic Liquids and Moisture[J]. Acta Photonica Sinica, 2026, 55(3):0355112
杨富龙,郭志涛,冯喆,等.基于双层金属超表面离子液体及水分检测双功能传感器[J].光子学报,2026,55(3):0355112

基于双层金属超表面离子液体及水分检测双功能传感器

杨富龙[1,2,3],郭志涛[1],冯喆[1],魏金艳[1],崔梦瑶[1],齐雨晴[1],王玉瑞[1]
(1 兰州理工大学 微电子现代产业学院,兰州 730050)
(2 兰州理工大学 自动化与电气工程学院,兰州 730050)
(3 兰州理工大学 酒泉先进技术研究院,兰州 730050)

摘 要:提出了一种基于双层金属谐振单元的超表面微波传感器。传感器由双层金属谐振单元、开放式样品架和全覆铜底板三层结构组成,双层谐振提高了传感器的灵敏度,开放式样品架设计便于样品装载与检测,全覆铜底板提升了电磁屏蔽性能。仿真与实验结果表明,在工作频段内,传感器对不同种类的离子液体表现出不同的特征频率响应,不同种离子液体之间的最大频率偏移量可达490 MHz,检测灵敏度达到185.42 MHz/ε′。对于含微量水分的1-乙基-3-甲基咪唑四氟硼酸盐溶液([EMIm][BF_4]),水分含量从0增加到10%时,可产生180 MHz的频率偏移量。该传感器具有结构紧凑、制作工艺简单等技术优势,为离子液体质量监测提供了高效方案。

关键词:超表面;传感器;离子液体;水分检测;微量检测
中图分类号:O436 **文献标识码**:A **doi**:10.3788/gzxb20265503.0355112

0 引言

近年来,离子液体作为一类由有机阳离子(如咪唑、吡啶和哌啶)与无机或有机阴离子(如卤素阴离子、四氟硼酸根和六氟磷酸根等)构成的有机熔融盐,已成为多个领域的研究热点。该类物质可在较宽的温度范围内(-90~-300 ℃)保持液态[1-3],并具备热稳定性好、电导率高、蒸汽压低、溶解度范围宽、可设计性强等许多优异性能[4-8],因而在电化学、催化反应、储能、生物化学及生物医学等领域具有广泛的应用潜力。在此背景下,实现离子液体的准确种类区分与介电常数测量,对深入理解其介电特性、优化电子器件以及开发新型功能材料具有重要意义[9]。然而,传统的表征方法如传统分析方法主要包括红外光谱(Infrared Spectroscopy, IR)、核磁共振波谱(Nuclear Magnetic Resonance, NMR)、质谱(Mass Spectrometry, MS)[10,11]以及同轴探测法等[12],通常依赖大型精密仪器,存在操作复杂、成本高、测量周期长等局限。此外,离子液体易吸湿的特性对储存纯度和测量准确性提出了更高要求。目前常用的水分检测方法如卡尔·费休法[13]、氮气吸附法[14]、干燥法、红外光谱法[15]、热重分析法等,同样面临设备昂贵、流程繁琐等挑战。因此,开发具备快速响应、高灵敏度、非破坏性及低成本优势的新型检测技术,已成为离子液体表征与鉴别中亟待解决的关键问题。

在此背景下,超表面(Metasurface)作为一种新型二维人工材料[16-18],凭借其亚波长结构单元对电磁波振幅、相位与偏振的精确调控能力[19-23],为高灵敏度传感提供了新的技术路径。该类传感器兼具优异的设计自由度与微型化潜力,能实现对待测物环境信号的非接触、快速响应检测,在物理、化学及生物传感中已展现

基金项目:甘肃省重大科技项目(25ZDGE003、25ZDWA001、25ZDGE0004、25ZDGA005),联合科研基金一般项目(24JRRA829),甘肃省重点研发计划——工业项目(25YFGA033),甘肃省教育厅青年博士基金项目(2024QB-036)
第一作者(通讯作者):杨富龙,yangfulong1982@126.com
收稿日期:2025-09-11;**录用日期**:2025-11-11

出显著优势[24-28]。具体应用研究显示，多种超表面结构已在传感检测中取得成效。例如，ZHANG Y等[29]采用交叉谐振器的超表面传感器，实现了谷物质量的无损、非接触测量；TIWARI N K等[30]利用蚀刻在喇叭形传输线顶部的双互补开口环谐振器(Complementary Split-Ring Resonator, CSRR)组成的超表面传感器，实现了区分材料的真伪；在介电参数测量方面，BAGCI F等[31]提出的如双“H”的基于双波段超表面传感器可用于测量乙醇甲醇二元混合物的复介电常数；袁婷婷等[32]基于对称开口环结构设计的太赫兹超表面微结构器件，其折射率灵敏度达到196 GHz/RIU，并成功应用于呋喃唑酮和呋喃妥因溶液的痕量检测。此外，ZHANG X等[33]通过微带传输线耦合两个螺旋谐振器和S形微流通道的超表面传感器实现了醇类水溶液的传感；ZHOU H等[34]结合对称双裂缝谐振器(Double Split-Ring Resonator, DSRR)与蜿蜒微流体通道的超表面传感器，实现了化学品介电特性的多波段传感；ZUBIN C等[35]设计的超表面传感器通过包含两个在磁性LC谐振器的开放喇叭形微带贴片来表征食用油的复介电常数。然而，上述基于微带传输线的传感器在测量过程中会受到周围的电磁干扰[36]而文献[35]提出的传感器会与样品直接接触，限制了测量精度并可能引起污染。

本文设计了一种基于介质基板集成双层金属谐振结构的超表面微波传感器，用于实现不同种类及不同水分含量离子液体的检测。该传感器通过结合理论分析、数值仿真和实验验证，实现了对六种离子液体种类的准确区分与对离子液体中微量水分含量的精确检测。所设计的超表面传感器结构新颖、性能优异、检测方法简便，具有无标记、非接触、非侵入等特点，并且其价格低廉，易于制备与集成。本研究为离子液体表征和纯度检测提供了一种全新的技术方案，在离子液体研究与工业应用中具有重要价值。

1 结构与设计

1.1 传感器原理及设计

超表面传感器的核心原理可将其建模为一个谐振系统，其共振特性(如频率、相位和振幅)对环境介电常数的变化具有高度敏感性。因此，传感器设计的关键在于主动构造并调控此类共振模式，从而建立共振参数与待测物物理特性之间的定量或定性映射关系。当待测物覆盖于传感器表面时，会与结构周围局域增强的电磁场发生强烈相互作用，导致共振行为发生显著变化。在共振频率处，超表面单元与入射波实现最佳耦合，能量被高效局域在结构内部。该局域能量可能以多种途径耗散或散射：包括被金属结构的欧姆损耗吸收、散射至非传播型衍射级次，或以反相方式重新辐射至远场。对于反射型结构，强烈的能量吸收与非前向散射将造成沿入射方向反射能量的显著降低，进而在反射谱或透射谱中形成明显的共振凹陷。

本文设计的超表面传感器结构如图1(a)所示，传感器的单元结构采用三层设计：上层为集成双金属谐振图案的基板，中层为开放式样品架用于盛载待测物，下层则采用全覆铜底板构成完整电磁屏蔽结构。基板

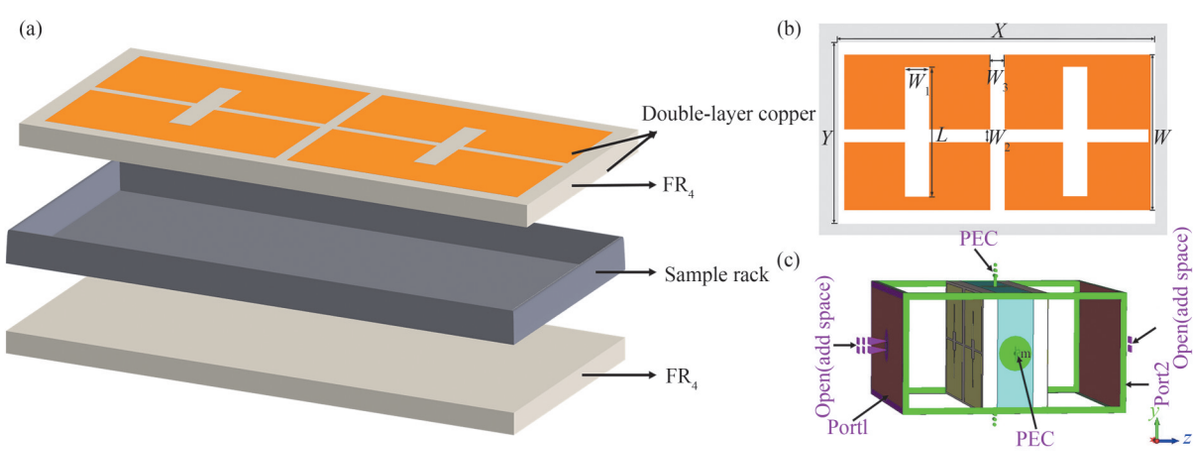

图1 超表面传感器示意结构图。(a)单元结构图；(b)金属谐振图案；(c)传感器设计：PEC-PEC开放边界条件

Fig. 1 Schematic structure of metasurface sensor. (a) Unit cell structure; (b) Metal resonant pattern; (c) Sensor design: PEC-PEC open boundary conditions

采用印刷电路板基板材料（Flame Retardant 4，FR_4），介电常数为4.3，损耗角正切为0.025，厚度为1.6 mm；同时，基板长宽设计为28.5 mm×13 mm，而HD-84WCAN波导的横截面尺寸为28.5 mm×13.5 mm，二者尺寸适配，因此其与HD-84WCAN波导兼容。基板上覆有图1(b)所示的铜图案，其电导率为5.8×10^8 S/m，厚度为50 μm。在电磁边界条件设置方面，考虑到波导侧壁的金属特性，在Z轴方向施加垂直入射的电磁激励，而在X轴和Y轴方向则设定为理想电导体边界，以准确模拟实际波导环境，具体如图1(c)所示。此外，本文为了在相关频率区域获得最高的频移和最佳的灵敏度性能，通过大量的参数研究，确定了设计参数的最佳值，并在表1中列出了相关几何参数。

表1　超表面传感器结构图参数表

Table 1　Parameter table of metasurface sensor structure

Parameter	Value/mm	Parameter	Value/mm
X	28.5	Y	13
W	12	L	8
W_1	0.4	W_2	0.2
W_3	1		

1.2　模型制作及测量

为验证传感器设计的可行性，采用高频PCB工艺在1.6 mm厚的FR_4基板上制备了超表面传感器。传感器采用双层谐振单元，分别位于基板上下层，结构简化且检测灵敏度显著提升。测量时，待测物置于样品架中，实现非接触式检测，避免样品污染并确保传感器的长期稳定性与可靠性。实验时，首先使用移液管将待测物质注入样品架，随后将传感器放置于波导装置中心进行实验测量。图2(a)展示了所设计的超表面传感器的实物照片；图2(b)为采用聚四氟乙烯材料加工的样品架及其几何参数示意图，其中样品架外部高度（H_{out}）为4 mm，用于容纳待测物质的内部宽度（W_{in}）为11.5 mm，内部长度（L_{in}）为27 mm，内部高度（H_{in}）为3 mm。此外，样品架外部宽度（W_{out}）为13 mm，外部长度（L_{out}）为28.5 mm，该尺寸不仅完全覆盖了金属超表面，而且与HD-84WCAN波导完全匹配。图2(c)为波导内部传感器结构的俯视图，图2(d)展示了实验所用的HD-84WCAN矩形波导，图2(e)为完整的实验测量系统布置图。

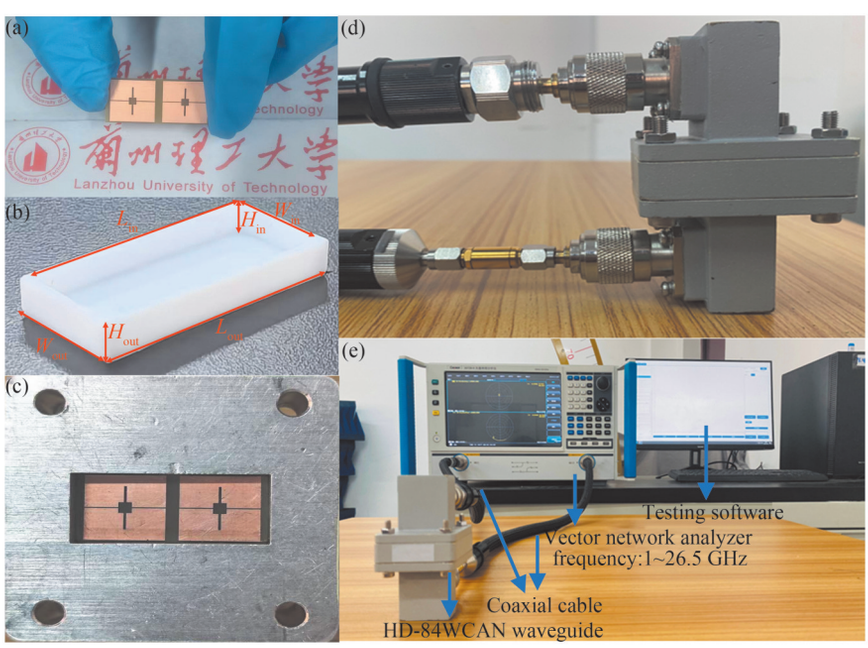

图2　实验效果图。(a)传感器实物图；(b)样品架；(c)；波导内传感器俯视图；(d)；矩形波导装置；(e)整体实验测量装置

Fig. 2　Overall experimental effect diagram. (a) Photograph of the fabricated sensor; (b) Sample holder; (c) Top view of the sensor inside the waveguide; (d) Rectangular waveguide assembly; (e) Overall experimental setup for measurement

2 机理分析

2.1 超表面传感器的表征

在传感器表征实验前，首先对超表面传感器的光谱响应进行了系统测量，并将实验结果与仿真数据进行了对比分析。测量采用如图2(e)所示的HD-84WCAN型波导系统，其几何尺寸与本文设计的超表面传感器保持一致。实验过程中，采用Ceyear 3672B-S矢量网络分析仪及配套波导测试装置，在7～10 GHz频段内精确测量了系统的散射参数(*S*参数)。

为研究超表面传感器对电磁响应的调控能力，基于电磁仿真软件对比分析了7～10 GHz频段内加载与未加载离子液体[EMIm][BF_4]时的反射特性(S_{11}参数)，结果如图3所示。在未加载样品时，传感器呈现双谐振特性，谐振峰分别位于8.98 GHz(－4 dB)与9.69 GHz(－8 dB)；而加载离子液体后，因该介质的介电特性与超表面相互作用，系统在8.37 GHz处产生显著的谐振吸收(－19 dB)。实验结果表明，离子液体的引入不仅改变了传感器的原有谐振模式，还通过介电调控使系统产生了更强的电磁响应，证实了该超表面传感器具备优异的介质敏感特性与电磁调控能力。

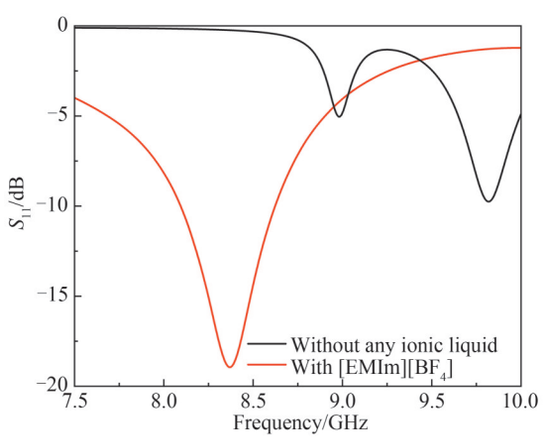

图3 样品架装载和不装载[EMIm][BF_4]离子液体的超表面传感器反射光谱仿真图

Fig. 3 Simulation diagrams of reflection spectra for metasurface sensors with and without [EMIm][BF_4] ionic liquid loaded in the sample holder

为深入探究超表面传感器的工作机理，本文从电磁场与表面电流耦合的角度揭示了结构谐振的物理本质。在电磁波激励下，其独特的超表面结构会产生强烈的电磁响应，形成特定的电流分布模式。传感器结构单元可等效为LC谐振回路，其谐振特性源于电感与电容的能量动态平衡。该结构对周围介质环境表现出高度敏感性：当被测样品与超表面相互作用时，原有电磁场分布将发生改变，引起谐振频率产生特征偏移，偏移幅度与传感器灵敏度密切相关。基于上述原理，通过电磁仿真对比分析了加载[EMIm][BF_4]离子液体前后的表面电流分布变化。图4仿真结果表明，箭头所示的电流方向与颜色表征的强度分布均发生显著变化。该变化源于谐振腔边界场区域的重新分布，即介质环境的变化直接影响谐振腔边缘场的分布密度。边缘场对介质负载的敏感性，为实现样品复介电常数的非接触测量的奠定了物理基础。

进一步观察未添加离子液体的表面电流分布变化情况。图4(a)与(b)展示了8.98 GHz频率处上下两层的表面电流分布，图4(c)与(d)对应9.69 GHz频率处的分布。可见表面电流主要集中在金属图案边缘，且上下两层电流方向相反，电流密度存在差异，从而形成不同的谐振，在S_{11}反射图谱上表现为在8.98 GHz与9.69 GHz处出现两个独立谐振峰。对比加载离子液体前后在各自谐振频率下的表面电流分布变化，如图4(c)～(f)所示，在9.69 GHz处未加载[EMIm][BF_4]时，金属图案边缘的表面电流如箭头所示形成闭环并呈现集中状态；加载[EMIm][BF_4]后，由于其吸收电磁波特性，导致电磁波能量的吸收与衰减均显著增大，表面电流分布受到了抑制，表面电流强度明显减弱。上述结果表明，离子液体的介电特性改变了电场与表面电流的分布，从而破坏了原有电磁谐振状态，使传感器的电磁响应特性发生重构。同时，模拟所得表面电流分布也证明，在谐振频率下该结构中存在产生谐振的电偶极子。

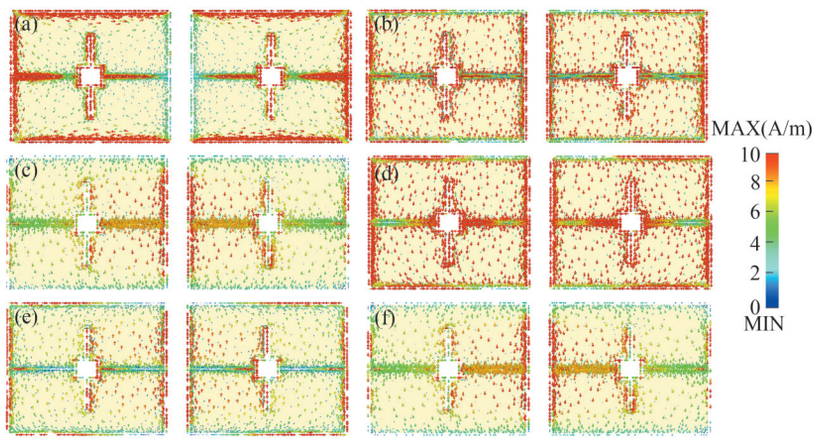

图4　表面电流分布图。(a)(d)未添加离子液体上下层表面电流分布图；(e)(f)添加离子液体上下层表面电流分布图

Fig. 4　Surface current distribution diagram. (a) (d) Surface current distributions on the top and bottom layers without ionic liquid; (e)(f) Surface current distributions on the top and bottom layers with ionic liquid

2.2　等效电路模型

为深入探究超表面传感器的工作机理并验证数值模拟结果的准确性，本文基于超表面传感器的金属单元结构特征及其在电磁场作用下的物理响应特性，分析电磁感应现象与电子运动规律，提取了传感器的等效电路参数，建立完整的等效电路模型（Equivalent Circuit Model，ECM），该模型为理解超表面传感器的电磁响应机制提供了理论依据。在等效电路模型中，将FR_4基底等效为传输线[37]，Z_1表示其特性阻抗，Z_0表示超表面结构与波导输入/输出端口之间的特性阻抗。上下两层对称分布的金属谐振图案分别等效为$R-L-C$电路；由于二者采用相同材料与结构，因此它们的等效电路保持一致。在电磁波激励下，上下金属图案之间会引入相互耦合电感L_3和L_4。此外，由于上下两层的对称金属谐振图案的表面电流方向对称，自由电子在其间振荡形成耦合电容C_3。基于上述分析所构造的等效电路如图5(a)所示，电路仿真与电磁仿真得

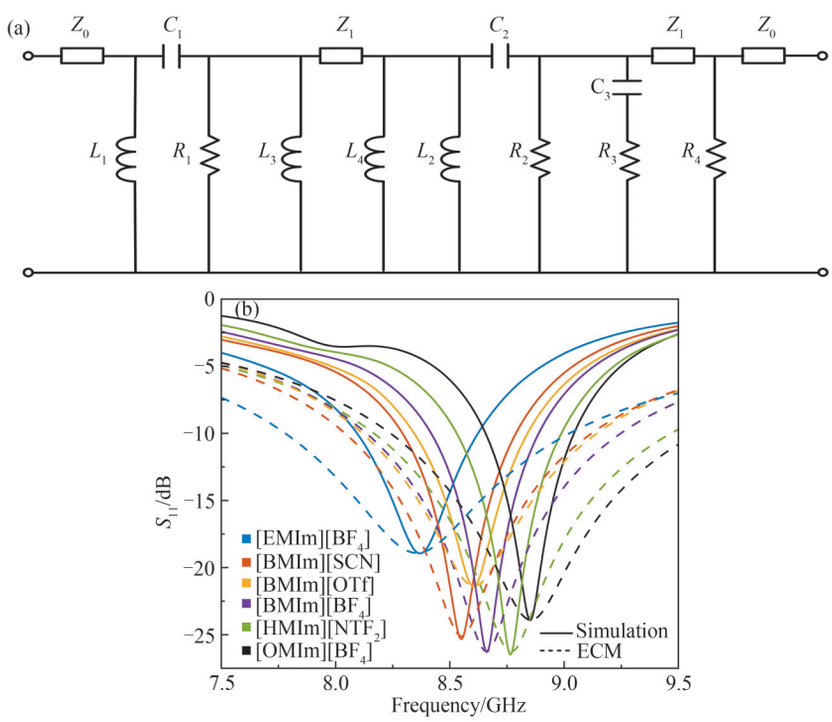

图5　等效电路模型图。(a)等效电路图；(b)电磁仿真与电路仿真图

Fig. 5　Equivalent circuit model diagram. (a) Equivalent circuit model; (b) Comparison of full-wave electromagnetic simulation and circuit simulation results

到的S_{11}如图5(b)所示。等效电路参数设置为：Z_0=377 Ω，Z_1=181.806 Ω，R_1=R_2=10 000 Ω，L_1=L_2=L_3=L_4=5 nH，C_1=C_2=0.09 pF。

当样品架加载被测离子液体时，其介电损耗会引入附加电阻R_3，同时其介电色散特性也会影响传感器的等效电容。为准确表征这一效应，在等效电路仿真中通过数值优化方法对R_3与C_3进行参数调整，结果如图5(b)所示。对比不同离子液体样品的电磁仿真与等效电路仿真结果，并分析加载样品时各电路元件参数的变化规律，发现两者具有良好的一致性，从而验证了所建电路模型的可靠性。需指出的是，电路模型的S参数曲线与电磁仿真结果存在轻微偏差，主要源于建模过程中未充分考虑某些寄生参数的影响[38]。

3 实验结果和讨论

3.1 离子液体的鉴别

选取[EMIm][BF_4]、1-丁基-3-甲基咪唑硫氰酸([BMIm][SCN])、1-丁基-3-甲基咪唑三氟甲磺酸盐([BMIm][OTf])、1-丁基-3-甲基咪唑四氟硼盐([BMIm][BF_4])、1-己基-3-甲基咪唑双(三氟甲磺酰)亚胺盐([HMIm][NTF_2])和1-辛基-3-甲基咪唑四氟硼酸盐([OMIm][BF_4])六种代表性离子液体作为被测样品，分别置于样品架中，采用S_{11}型矢量网络分析仪测量其反射光谱，结果如图6所示。为建立S_{11}参数与离子液体复介电常数之间的定量关系并验证传感器测量可重复性，实验设计如下：共进行两组平行测试，每组分别对六种离子液体各重复测量五次；第一组数据用于构建定量模型，第二组数据用于模型验证与性能评估。实验测得的6种离子液体的反射光谱如图6所示，测量结果表明当样品架中的待测样品从[EMIm][BF_4]更换为[OMIm][BF_4]时，反射谱的谐振峰位置从8.37 GHz偏移至8.86 GHz，产生了显著的490 MHz频移现象。这种频率响应特性的变化源于不同离子液体所具有的独特复介电常数特性。当超表面传感器与不同离子液体相互作用时，会激发出特征各异的电磁谐振响应模式，具体表现为反射谱中谐振峰位置的系统性偏移。通过对图6所示反射光谱的深入分析，可以从三个关键特征参数进行定量表征：谐振频率(反映介电特性)、Q因子(表征谐振锐度)以及振幅(指示能量损耗)。上述特征参数的提取为后续建立离子液体介电性能与电磁响应之间的定量关系奠定了基础。

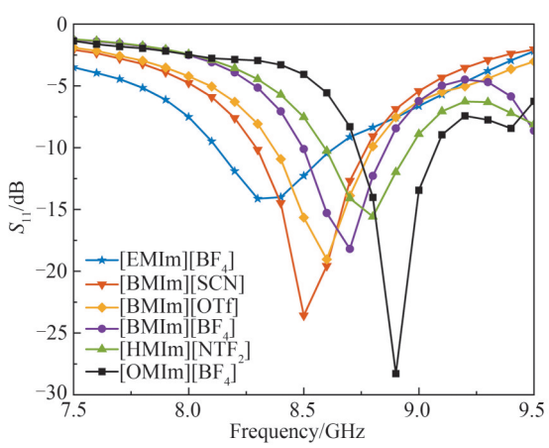

图6 六种不同离子液体实验测量反射光谱

Fig. 6 Experimental measurement reflection spectra of six different ionic liquids

采用探针法测得6种离子液体在谐振频率下的复介电常数值列于表2。提取图6中各反射曲线的谐振频率并分析其变化趋势(图7(a))，结果表明谐振频率随着离子液体的种类不同呈现近似线性的变化规律，且与复介电常数的变化趋势相反。为量化频率响应特性，本文以添加的样品[EMIm][BF_4]的谐振频率作为基准频率，将其他离子液体的谐振频率相对于该基准的偏移量作为主要传感指标。如图7(a)所示，共振频率和频率偏移均随着离子液体种类呈现出大致的线性增长趋势。品质因数Q值的变化规律如图7(b)所示，其随离子液体类型呈现非线性波动。用于构建矩阵的反射谱参数—频率偏移量Δf与Q值变化量ΔQ随离子

液体类型变化的趋势如图7(c)所示，随着复介电常数实部的减小，谐振频率偏移量与Q值变化量总体呈现上升态势。

表 2　离子液体介电常数与共振频率变化的关系

Table 2　Relationship between dielectric constant of ionic liquids and resonance frequency shift

Sample	ε'	ε''	Frequency/GHz
[EMIm][BF_4]	8.05	8.04	8.37
[BMIm][SCN]	7.46	5.18	8.55
[BMIm][OTf]	6.60	4.78	8.60
[BMIm][BF_4]	6.33	3.86	8.66
[HMIm][NTF_2]	5.39	2.35	8.77
[OMIm][BF_4]	5.03	1.86	8.86

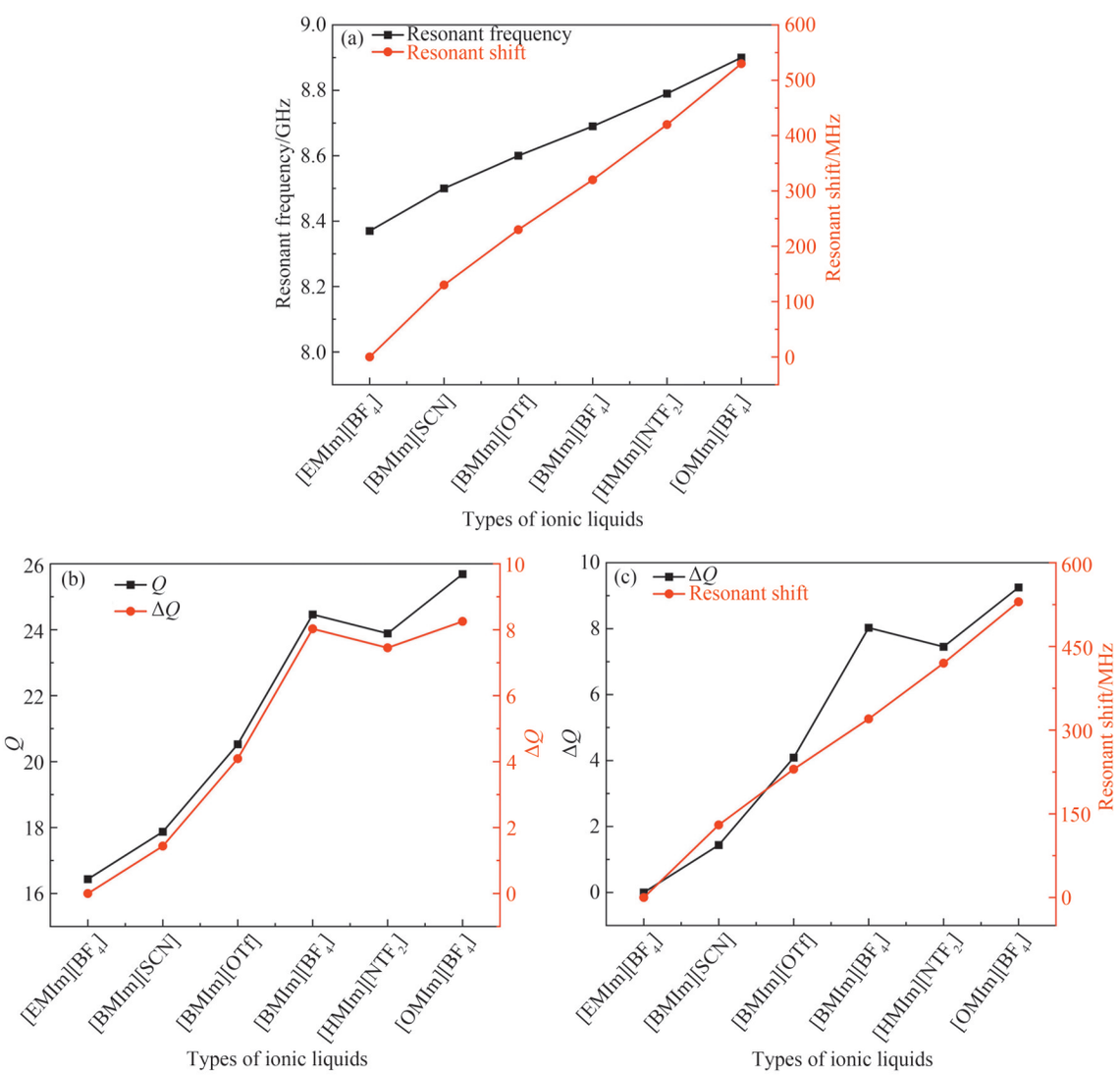

图 7　实验测量结果分析图。(a)谐振频率与频移变化；(b)Q因子和Q因子变化；(c)频移与Q因子变化

Fig. 7　Analysis diagrams of experimental measurement results. (a) Resonant frequency and frequency shift; (b) Q-factor and its variation; (c) Frequency shift versus Q-factor variation

基于最小二乘法来建立相应的数学模型，以定量描述上述六种离子液体的复介电常数与谐振曲线之间的相互关系。换言之，待测样品的复介电常数与谐振频率变化量及Q因子变化量相关，而谐振频率与Q因子变化量又可以根据待测样品的复介电常数进行描述，这种关联可以通过式(1)的矩阵来表达，有

$$\begin{bmatrix}\Delta f_0\\ \Delta Q\end{bmatrix}=\begin{bmatrix}m_{11}\ m_{12}\\ m_{21}\ m_{22}\end{bmatrix}\begin{bmatrix}\Delta\varepsilon'_{\text{sample}}\\ \Delta\varepsilon''_{\text{sample}}\end{bmatrix}\tag{1}$$

式中，

$$\Delta f_0=f_{\text{sample}}-f_{\text{reference}}\tag{2}$$

$$\Delta Q=Q_{\text{sample}}-Q_{\text{reference}}\tag{3}$$

$$\Delta\varepsilon=\varepsilon_{\text{sample}}-\varepsilon_{\text{reference}}\tag{4}$$

在式(1)中，m_{11}，m_{12}，m_{21}，m_{22}是以[EMIm][BF_4]作为参考的未知系数，$\Delta\varepsilon$(包括复介电常数的实部和虚部)是复介电常数的变化量，Δf是谐振频率的变化量，ΔQ是Q因子的变化量。从表2计算的复介电常数的变化量、图6中提取的谐振频率的变化量及Q因子变化量。矩阵$\boldsymbol{Y}_1$、$\boldsymbol{Y}_2$、X定义为

$$\boldsymbol{Y}_1=\begin{bmatrix}\Delta f_{[\text{EMIm}][BF_4]}\\ \Delta f_{[\text{BMIm}][\text{SCN}]}\\ \Delta f_{[\text{BMIm}][\text{OTf}]}\\ \Delta f_{[\text{BMIm}][BF_4]}\\ \Delta f_{[\text{HMIm}][NTF_2]}\\ \Delta f_{[\text{OMIm}][BF_4]}\end{bmatrix}=\begin{bmatrix}0\\ 0.13\\ 0.23\\ 0.32\\ 0.42\\ 0.53\end{bmatrix}$$

$$\boldsymbol{Y}_2=\begin{bmatrix}\Delta Q_{[\text{EMIm}][BF_4]}\\ \Delta Q_{[\text{BMIm}][\text{SCN}]}\\ \Delta Q_{[\text{BMIm}][\text{OTf}]}\\ \Delta Q_{[\text{BMIm}][BF_4]}\\ \Delta Q_{[\text{HMIm}][NTF_2]}\\ \Delta Q_{[\text{OMIm}][BF_4]}\end{bmatrix}=\begin{bmatrix}0\\ 1.43868\\ 4.08931\\ 8.02687\\ 7.45168\\ 9.25119\end{bmatrix}$$

$$\boldsymbol{X}=\begin{bmatrix}\Delta\varepsilon'_{[\text{EMIm}][BF_4]} & \Delta\varepsilon''_{[\text{EMIm}][BF_4]}\\ \Delta\varepsilon'_{[\text{BMIm}][\text{SCN}]} & \Delta\varepsilon''_{[\text{BMIm}][\text{SCN}]}\\ \Delta\varepsilon'_{[\text{BMIm}][\text{OTf}]} & \Delta\varepsilon''_{[\text{BMIm}][\text{OTf}]}\\ \Delta\varepsilon'_{[\text{BMIm}][BF_4]} & \Delta\varepsilon''_{[\text{BMIm}][BF_4]}\\ \Delta\varepsilon'_{[\text{HMIm}][NTF_2]} & \Delta\varepsilon''_{[\text{HMIm}][NTF_2]}\\ \Delta\varepsilon'_{[\text{OMIm}][BF_4]} & \Delta\varepsilon''_{[\text{OMIm}][BF_4]}\end{bmatrix}=\begin{bmatrix}0 & 0\\ -0.62608309 & -2.89935285\\ -1.50244282 & -3.3092843\\ -1.77794916 & -4.23595943\\ -2.72498328 & -5.13882781\\ -3.07912394 & -6.23608038\end{bmatrix}$$

将实验数据代入计算得到的系数矩阵为

$$\begin{bmatrix}m_{11} & m_{12}\\ m_{21} & m_{22}\end{bmatrix}=\begin{bmatrix}-0.1231 & -0.0206\\ -3.7295 & 0.3246\end{bmatrix}\tag{5}$$

用于估计复介电常数的数学模型可以通过该系数矩阵的逆矩阵来获得，即

$$\begin{bmatrix}\Delta\varepsilon'\\ \Delta\varepsilon''\end{bmatrix}=\begin{bmatrix}m_{11} & m_{12}\\ m_{21} & m_{22}\end{bmatrix}^{-1}\begin{bmatrix}\Delta f_{\text{sam}}\\ \Delta Q\end{bmatrix}=\begin{bmatrix}-2.7794 & -0.1764\\ -31.9345 & 1.0541\end{bmatrix}\begin{bmatrix}\Delta f_{\text{sam}}\\ \Delta Q\end{bmatrix}\tag{6}$$

为验证所建矩阵模型的普适性，在首次实验基础上采用相同测量方案，重新加载样品[EMIm][BF_4]并在不同时间段进行重复实验，以获取预测数据。通过对第二次实验数据进行特征提取，得到各样品谐振频率与Q值的变化情况，如图8(a)所示。与图7(c)结果相比，ΔQ仅出现微小差异，这个差异主要源于实验环境的误差。

将提取的Δf_{sample}和ΔQ值代入式(6)中，可计算出六种离子液体的复介电常数实部与虚部。估算结果如图8(b)所示。通过将估算数据与探针法在对应频率下的实测数据进行对比，复介电常数实部与虚部的估算值与测量值具有良好的一致性。由于建模数据和估算数据均以[EMIm][BF_4]为参照基准，该离子液体的复介电常数实部与虚部估算值与测量数据完全吻合。以复介电常数实部、虚部和谐振频率分别作为X、Y、Z构建三维分布图，如图8(c)所示。六种离子液体样品在三维空间中呈近似线性分布，且任意两种离子液体之间均不存在分布区域重叠现象，表明不同离子液体在介电特性空间中分布均匀。该结果表明，本文所构建的超表面传感器可以有效区分这六中不同类型的离子液体。

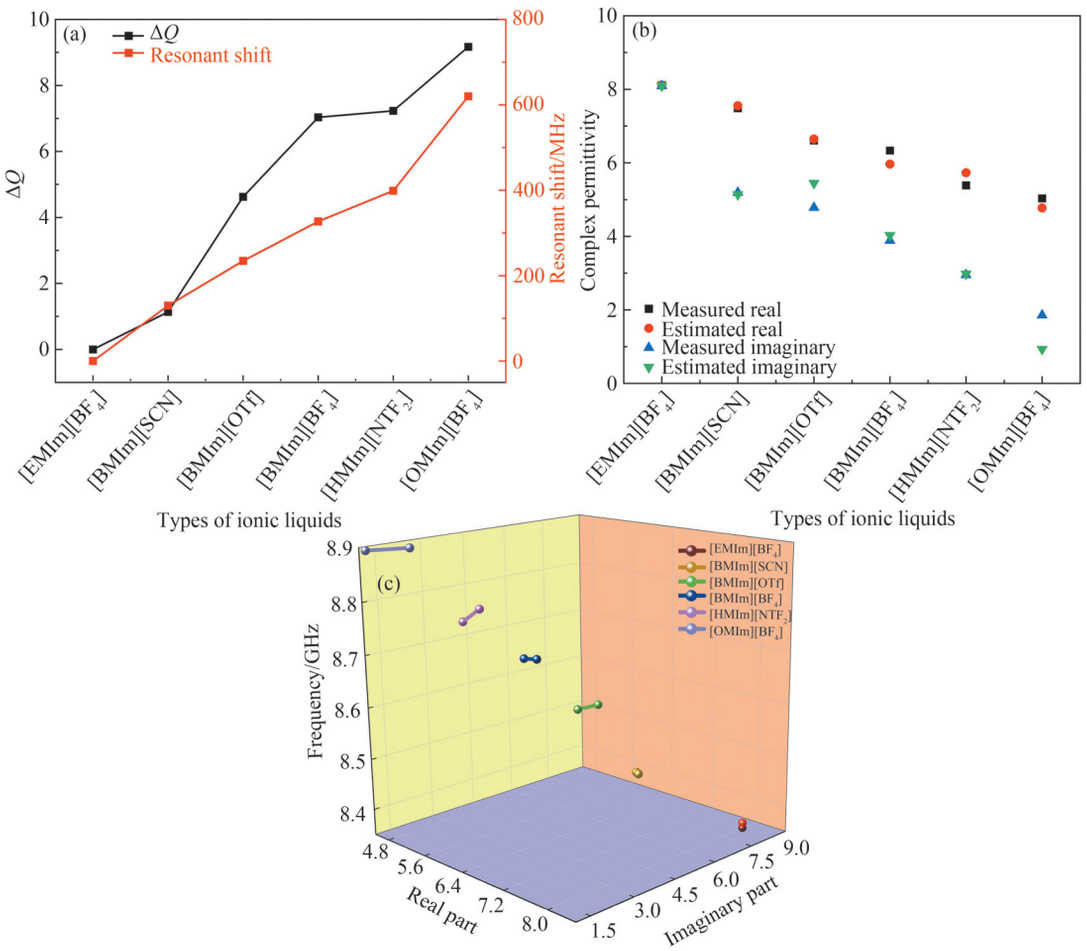

图8　实验结果分析图。(a)谐振频率与Q因子变化。(b)离子液体测量与估计复介电常数对比；(c)不同类型样品介电特性

Fig. 8　Experimental result analysis diagram. (a) Variations of resonant frequency and Q-factor; (b) Comparison of measured and estimated complex permittivity of the ionic liquid; (c) Dielectric properties of different sample types

3.2　离子液体水分检测

为评估传感器对微量水分检测的灵敏度，本文选取典型离子液体[EMIm][BF_4]作为检测对象，精确配比制备了不同含水量的测试样品。为避免水分比例过高影响检测特性，实验严格控制含水量，在10 mL [EMIm][BF_4]中分别掺入0.526 mL和1.111 mL纯净水，制得含水量为5%与10%的两种测试溶液。采用探针法精确测量了纯[EMIm][BF_4]及其含水溶液的复介电常数如图9(a)所示。其结果表明，不同含水量样

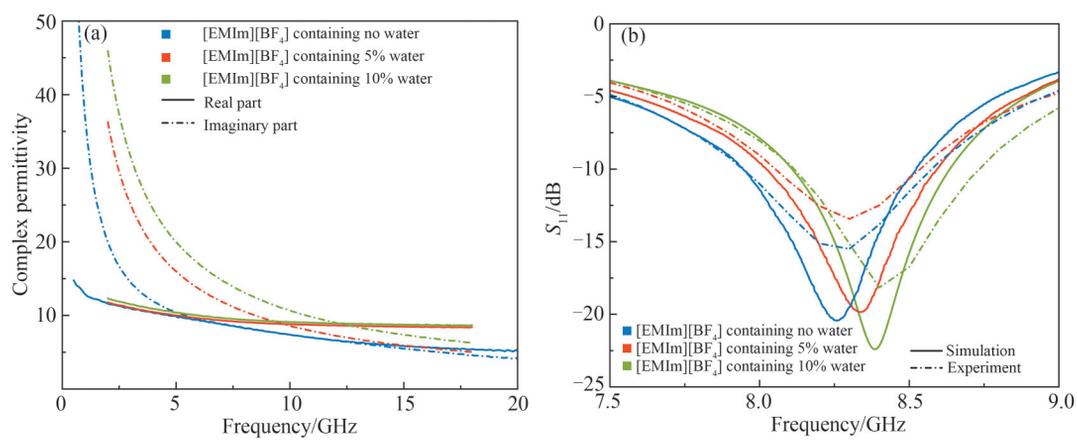

图9　离子液体水分检测实验图。(a)不同含水量样品复介电常数；(b)[EMIm][BF_4]及其水溶液实验与仿真反光谱

Fig. 9　Experimental diagram of water detection in ionic liquids. (a) Complex permittivity of samples with different water contents; (b) Experimental and simulated reflection spectra of [EMIm][BF_4] and its aqueous solutions

品之间的介电常数实部与虚部存在细微差异。仿真与实验结果如图9(b)所示，当含水量从0%增至10%时，反射谱谐振峰产生180 MHz的显著频移(8.22 GHz→8.40 GHz)。这一结果表明该传感器具备检测离子液体中ppm级水分变化的高灵敏度。

3.3 超表面传感器的性能分析

为了评估传感器性能，本文计算了所提出的传感器的灵敏度，并与近期发表的相关成果进行了对比分析。灵敏度采用文献[39]中式(7)所示关系式进行计算。

$$S=\frac{\Delta f}{\Delta \varepsilon'} \tag{7}$$

式中，

$$\Delta f=\left| f_{\text{sample}}-f_{[\text{EMIm}][\text{BF}_4]} \right| \tag{8}$$

$$\Delta \varepsilon'=\left| \varepsilon'_{\text{sample}}-\varepsilon'_{[\text{EMIm}][\text{BF}_4]} \right| \tag{9}$$

由于不同的研究者提出的传感器工作频率各异，且检测样品的复介电常数存在差异，因此，采用文献[40]给出的频率归一化公式(10)对灵敏度进行了标准化处理，以实现传感器的精确比较。

$$S_{\text{avg},f}(\%)=\frac{\Delta f}{f_0 \Delta \varepsilon'}\times 100\% \tag{10}$$

式中，f_0是超表面传感器中加载样品[EMIm][BF_4]时测量的谐振频率。

测量结果表明传感器的平均灵敏度为185.42 MHz/ε′，归一化灵敏度达21.9%。两次实验测量的平均灵敏度误差百分比为6.29%，该误差相对较小，差异主要源于实验环境的误差。将传感器的性能与近期相关研究进行了对比，结果如表2所示。研究表明，该传感器的灵敏度优于近期报道的大多数方案，且采用的基板为低成本常规FR_4电路板。总体而言，所提出的超表面传感器综合性能优异。

表2 离子液体介电常数与共振频率变化的关系

Table 2 Relationship between dielectric constant of ionic liquids and resonance frequency shift

Reference	f_r/GHz	S_{avg}(MHz/ε′)	$S_{\text{avg},f}$/%	ε′ range	Substrate
[41]	20	59.75	0.298	20～44.7	Quartz wafer
[42]	2.54	89.5	3.58	2.93～3.64	RO3010
[43]	3.364	165.33	4.915	1～2.9	Taconic TLY-5
[44]	3.2	92.86	2.9	11～81	Polycarbonate
[45]	3.67	25.3	0.73	5～20	Polycarbonate
	4.55	9.6	0.22		
This work	8.37	185.42	21.9	4～9	FR_4

4 结论

本文设计并验证了一种基于双层金属谐振单元的超表面微波传感器。通过采用FR4环氧树脂基板构建的三层结构，结合开放式样品架和全镀铜底板设计，传感器在8～9 GHz工作频段展现出卓越的检测性能，实现了对离子液体及其水分含量的非接触高精度检测。仿真与实验结果表明，该传感器对六种典型离子液体([EMIm][BF_4]、[BMIm][SCN]、[BMIm][OTf]、[BMIm][BF_4]、[HMIm][NTF_2]和[OMIm][BF_4])均具有不同的特征频率响应，最大频率偏移达490 MHz，检测灵敏度高达185.42 MHz/ε′。在离子液体水分检测方面，传感器对[EMIm][BF_4]溶液中0～10%的水分含量变化表现出良好的谐振响应，谐振频率偏移达180 MHz。本文设计的超表面传感器具有高灵敏度和良好的测量重复性，为离子液体纯度检测和变质监测提供了有效手段，在化工过程控制、危险环境监测等领域具有重要的应用前景。

参考文献

[1] LUO J, LIN F, YUAN J, et al. Application of ionic liquids and derived materials to high-efficiency and stable perovskite solar cells[J]. ACS Materials Letters, 2022, 4(9): 1684-1715.

[2] KIM JY, LEE JW, JUNG HS, et al. High-efficiency perovskite solar cells[J]. Chemical Reviews, 2020, 120(15): 7867-7918.

[3] DENG X, XIE L, WANG S, et al. Ionic liquids engineering for high-efficiency and stable perovskite solar cells[J]. Chemical Engineering Journal, 2020, 398: 125594.
[4] YE Y S, RICK J, HWANG B J. Ionic liquid polymer electrolytes[J]. Journal of Materials Chemistry A, 2013, 1(8): 2719-2743.
[5] ZHANG W X, GAO Y R, XUE R, et al. Liquid formulations based on ionic liquids in biomedicine[J]. Materials Today Physics, 2023, 30: 100925.
[6] CHEN Y, HAN X, LIU Z, et al. Thermal decomposition and volatility of ionic liquids: Factors, evaluation and strategies [J]. Journal of Molecular Liquids, 2022, 366: 120336.
[7] YANG F, GONG J, YANG E, et al. Microwave-absorbing properties of room-temperature ionic liquids[J]. Journal of Physics D: Applied Physics, 2019, 52(15): 155302.
[8] BUFFETEAU T, GRONDIN J, LASSEGUES JC. Infrared spectroscopy of ionic liquids: quantitative aspects and determination of optical constants[J]. Applied Spectroscopy, 2010, 64(1): 112-119.
[9] DAMODARAN K. Recent advances in NMR spectroscopy of ionic liquids[J]. Progress in Nuclear Magnetic Resonance Spectroscopy, 2022, 129: 1-27.
[10] BENNETT E L, SONG C, HUANG Y, et al. Measured relative complex permittivities for multiple series of ionic liquids [J]. Journal of Molecular Liquids, 2019, 294: 111571.
[11] WEI Q, SHU-YUE A, SHUAI C, et al. A method of measuring complex ermittivity of nonmagnetic materials and selecting its initial value based on iterative inversion[J]. Acta Physica Sinica, 2023, 72(7): 070601.
覃维, 安书悦, 陈帅, 等. 基于迭代反演的非磁性材料复介电常数测量及初值选取方法[J]. 物理学报, 2023, 72(7): 070601.
[12] ABDULKARIM Y I, DENG L, ALTINTAŞ O, et al. Metamaterial absorber sensor design by incorporating swastika shaped resonator to determination of the liquid chemicals depending on electrical characteristics[J]. Physica E: Low-dimensional systems and Nanostructures, 2019, 114: 113593.
[13] RADCHENKO O B, RADCHENKO D S, KONOVETS A I, et al. Water determination in aromatic sulfonyl chlorides using the Karl Fischer titration method: scope and limitations[J]. ChemistrySelect, 2022, 7(2): e202102749.
[14] PENG L, YIN T, SONG Z, et al. Superior ammonia nitrogen adsorption capacity and reusability biochar microsphere applied in live fish transportation[J]. Chemical Engineering Journal, 2025: 163261.
[15] VEGA-CASTELLOTE M, PÉREZ-MARÍN D, TORRES-RODRÍGUEZ I, et al. Implementing near infrared spectroscopy for the online internal quality and maturity stage classification of intact watermelons at industry level[J]. Spectrochimica Acta Part A: Molecular and Biomolecular Spectroscopy, 2025: 126254.
[16] MEI Zhonglei, ZHANG Li, CUI Tiejun. Research progress of electromagnetic metamaterials[J]. Science & Technology Review, 2016, 34(18): 27-39.
梅中磊, 张黎, 崔铁军. 电磁超材料研究进展[J]. 科技导报, 2016, 34(18): 27-39.
[17] TANG Wenxuan, CUI Tiejun. Development and Application of Electromagnetic Metamaterials[J]. Optoelectronic Technology, 2024, 44(2): 85-93.
汤文轩, 崔铁军. 电磁超材料的发展与应用[J]. 光电子技术, 2024, 44(2): 85-93.
[18] LIU Junfeng, LIU Shuo, FU Xiaojian, et al. Terahertz information metamaterials and metasurfaces[J]. Journal of Radars, 2018, 7(1): 46-55.
刘峻峰, 刘硕, 傅晓建, 等. 太赫兹信息超材料与超表面[J]. 雷达学报, 2018, 7(1): 46-55.
[19] QIU T, SHI X, WANG J, et al. Deep learning: a rapid and efficient route to automatic metasurface design [J]. Advanc Science, 2019, 6(12): 1900128.
[20] CAO L, YANG Z, XU Y J J O S, et al. Steering elastic SH waves in an anomalous way by metasurface [J]. Journal of Sound and Vibration ,2018, 418: 1-14.
[21] ZHANG Lei, LIU Shuo, CUI Tiejun. Theory and Applications of Electromagnetic Coding Metamaterials[J]. Chinese Optics, 2017, 10(1): 1-12.
张磊, 刘硕, 崔铁军. 电磁编码超材料的理论与应用[J]. 中国光学, 2017, 10(1): 1-12.
[22] CHEN Ying, ZHANG Min, DING Zhixin, et al. Microfluidic refractive index sensor based on all-dielectric metasurface [J]. Chinese Journal of Lasers, 2022, 49(6): 0613001.
陈颖, 张敏, 丁志欣, 等. 基于全介质超表面的微流体折射率传感器[J]. 中国激光, 2022, 49(6): 0613001.
[23] LIU Hai, REN Ziyan, CHEN Cong, et al. Design of multifunctional sensor based on fano resonance metasurface[J]. Chinese Journal of Lasers, 2023, 50(10): 1010001.
刘海, 任紫燕, 陈聪, 等. 基于 Fano 共振超表面的多功能传感器设计[J]. 中国激光, 2023, 50(10): 1010001.
[24] ZHU R, WANG J, HAN Y, et al. Virtual metasurfaces: reshaping electromagnetic waves in distance[J]. Photonics Research, 2023, 11(2): 203-211.
[25] LU X, GE H, JIANG Y, et al. A dual-band high-sensitivity THz metamaterial sensor based on split metal stacking ring

[J]. Biosensors, 2022, 12(7): 471.
[26] QI Meiqing. Regulation and application of electromagnetic waves by metamaterial lenses and metasurfaces[D]. Nanjing: Southeast University, 2016.
齐美清. 超材料透镜和超表面对电磁波的调控及应用[D]. 南京: 东南大学, 2016.
[27] DAI Junyan, CUI Tiejun. New mode of nonlinear metasurfaces: space-time-coding digital metasurfaces[J]. Physics, 2021, 50(5): 293-299.
戴俊彦, 崔铁军. 非线性超表面新模式: 时空编码数字超表面[J]. 物理, 2021, 50(5): 293-299.
[28] SUN Shulin, HE Qiong, ZHOU Lei. Electromagnetic Metasurfaces[J]. Physics, 2015, 44(06): 366-376.
孙树林, 何琼, 周磊. 电磁超表面[J]. 物理, 2015, 44(6): 366-376.
[29] ZHANG Y, ZHAO J, CAO J, et al. Microwave metamaterial absorber for non-destructive sensing applications of grain [J]. Sensors, 2018, 18(6): 1912.
[30] TIWARI NK, SINGH SP, AKHTAR MJ. Novel improved sensitivity planar microwave probe for adulteration detection in edible oils[J]. IEEE Microwave and Wireless Components Letters, 2018, 29(2): 164-166.
[31] BAGCI F, GULSU M S, AKAOGLU B. Dual-band measurement of complex permittivity in a microwave waveguide with a flexible, thin and sensitive metamaterial-based sensor[J]. Sensors and Actuators A: Physical, 2022, 338: 113480.
[32] YUAN Tingting, WU Jingwen, BO Yanhua, et al. Trace detection of nitrofuran drugs based on terahertz metasurface sensor[J]. Acta Optica Sinica, 2023, 43(7): 0717001.
袁婷婷, 吴靖文, 薄艳华, 等. 基于太赫兹超表面传感器的硝基呋喃类药物痕量检测[J]. 光学学报, 2023, 43(7): 0717001.
[33] ZHANG X, RUAN C, CAO Y. A dual-mode microwave sensor for edible oil characterization using magnetic-LC Resonators[J]. Sensors and Actuators A: Physical, 2022, 333: 113275.
[34] ZHOU H, HU D, YANG C, et al. Multi-band sensing for dielectric property of chemicals using metamaterial integrated microfluidic sensor[J]. Scientific Reports, 2018, 8(1): 14801.
[35] ZUBIN C, SHUYUN M, WEI M. Synthesis of chloroaluminate ionic liquids and use for olefin reduction in FCC gasoline [J]. Petroleum Science and Technology, 2007, 25(9): 1173-1184.
[36] XU Y, ZHANG R, ZHOU Y, et al. Tuning ionic liquid-based functional deep eutectic solvents and other functional mixtures for CO2 capture[J]. Chemical Engineering Journal, 2023, 463: 142298.
[37] BILOTTI F, TOSCANO A, VEGNI L, et al. Equivalent-circuit models for the design of metamaterials based on artificial magnetic inclusions[J]. IEEE transactions on microwave theory and techniques, 2007, 55(12): 2865-2873.
[38] HAN X, LIU K, ZHANG S, et al. CSRR metamaterial microwave sensor for measuring dielectric constants of solids and liquids[J]. IEEE Sensors Journal, 2024, 24(9): 14167-14176.
[39] BURAGOHAIN A, DAS G S, BERIA Y, et al. Highly sensitive DS-CSRR based microwave sensor for permittivity measurement of liquids[J]. Measurement Science and Technology, 2023, 34(12): 125134.
[40] BURAGOHAIN A, MOSTAKO A T T, DAS G S. Low-cost CSRR based sensor for determination of dielectric constant of liquid samples[J]. IEEE Sensors Journal, 2021, 21(24): 27450-27457.
[41] CHRETIENNOT T, DUBUC D, GRENIER K. A microwave and microfluidic planar resonator for efficient and accurate complex permittivity characterization of aqueous solutions[J]. IEEE Transactions on Microwave Theory and Techniques, 2012, 61(2): 972-978.
[42] SU L, MATA-CONTRERAS J, VÉLEZ P, et al. Analytical method to estimate the complex permittivity of oil samples [J]. Sensors, 2018, 18(4): 984.
[43] VARSHNEY P K, KAPOOR A, AKHTAR M J. Highly sensitive ELC resonator based differential sensor[J]. IEEE Transactions on Instrumentation and Measurement, 2021, 70: 1-10.
[44] GULSU M S, BAGCI F, CAN S, et al. Metamaterial-based sensor with a polycarbonate substrate for sensing the permittivity of alcoholic liquids in a WR-229 waveguide[J]. Sensors and Actuators A: Physical, 2020, 312: 112139.
[45] BAO J Z, SWICORD M L, DAVIS C C. Microwave dielectric characterization of binary mixtures of water, methanol, and ethanol[J]. The Journal of chemical physics, 1996, 104(12): 4441-4450.

Double-layered Metasurface-based Dual-function Sensor for Detecting Ionic Liquids and Moisture

YANG Fulong[1,2,3], GUO Zhitao[1], FENG Zhe[1], WEI Jinyan[1], CUI Mengyao[1], QI Yuqing[1], WANG Yurui[1]

(1 *School of Microelectronics and Modern Industry, Lanzhou University of Technology, Lanzhou* 730050, *China*)
(2 *School of Automation and Electrical Engineering, Lanzhou University of Technology, Lanzhou* 730050, *China*)
(3 *Jiuquan Advanced-Technology Research Institute, Lanzhou University of Technology, Lanzhou* 730050, *China*)

Abstract: Ionic liquids, as a new type of molten salts with high thermal stability, low vapor pressure, and strong designability, have important application value in cutting-edge fields such as electrochemistry, catalytic synthesis, and biomedicine. However, the accuracy and efficiency of ionic liquid type identification still need to be continuously explored and optimized. Traditional characterization methods, such as infrared spectroscopy and nuclear magnetic resonance, usually rely on large precision instruments, which have limitations such as complex operating procedures, high equipment costs, and long analysis cycles. At the same time, the inherent strong hygroscopicity of ionic liquids makes the control of sample purity more stringent, and existing moisture detection methods find it difficult to achieve rapid and precise measurement. Against this background, metasurfaces, as two-dimensional artificial materials that can flexibly control the amplitude, phase, and polarization of electromagnetic waves, provide a new technical path for the development of high-performance sensing technologies. This type of structure has both high sensitivity and non-contact detection advantages, and has shown significant potential in dielectric property analysis and substance identification. However, existing metasurface sensors still have certain limitations in practical applications, such as being easily affected by external electromagnetic interference or requiring direct contact with samples. These issues not only reduce measurement accuracy but may also cause sensor contamination, thereby limiting their widespread application in practical scenarios.

Aiming at the technical bottlenecks of ionic liquid type identification and moisture content detection mentioned above, this paper proposes a metasurface microwave sensor based on a dielectric substrate integrated with a double-layer metal resonant structure. The sensor converts the dielectric properties of ionic liquids into significant changes in resonant frequency shift and resonance linearity through its unique electromagnetic field localization and enhancement mechanism, providing a new way to achieve rapid and precise sensing analysis. To deeply study the working mechanism of the sensor, this study adopted a multi-level research method: from the physical mechanism level, the formation and energy distribution of electromagnetic resonance were intuitively presented through surface current distribution analysis; from the model construction level, the physical structure was transformed into circuit parameters through equivalent circuit analysis, and the regulation law of resonant frequency was quantitatively revealed; from the performance prediction level, the electromagnetic response characteristics of the sensor were accurately obtained through full-wave numerical simulation, and the structure was optimized; from the final verification level, experimental tests confirmed that the sensor can not only accurately distinguish six different types of ionic liquids but also achieve high-precision detection of trace moisture content.

Before conducting experimental characterization, this study first compared and analyzed the reflection characteristic changes of the sensor before and after loading ionic liquids in the 7~10 GHz frequency band based on electromagnetic simulation software. The simulation results show that the introduction of ionic liquids not only changed the original resonant mode of the sensor but also induced a stronger electromagnetic response through the dielectric regulation mechanism, thereby verifying that the metasurface sensor has excellent dielectric sensitivity and electromagnetic regulation capabilities. Subsequently, six representative ionic liquids were selected as the measured samples for actual measurement analysis. The experimental measurement results show that when the sample to be tested in the sample holder is changed from [EMIm][BF_4] to [OMIm][BF_4], the resonant peak position of the reflection spectrum shifts from 8.37 GHz to 8.86 GHz, resulting in a significant frequency shift of 490 MHz. Calculations show that the sensor's average sensitivity to dielectric constant changes can reach 185.42 MHz/ε'. In addition, this study systematically evaluated the sensor's ability to detect trace moisture

content. Experimental data show that when the water content increases from 0% to 10%, the resonant peak of the reflection spectrum shows a significant frequency shift of 180 MHz (8.22 GHz→8.40 GHz), proving that the sensor can effectively detect moisture changes in ionic liquids at the ppm level.

In summary, this paper successfully designed and verified a metasurface microwave sensor based on a double-layer metal resonant unit. By using a three-layer structure constructed with an FR4 epoxy resin substrate, combined with an open sample holder and a fully copper-plated bottom plate design, the sensor exhibits excellent detection performance in the 7～10 GHz working frequency band, achieving non-contact and high-precision detection of ionic liquid types and their moisture content. Simulation and experimentalresults show that the sensor has different characteristic frequency responses for six typical ionic liquids (including [EMIm][BF_4], [BMIm][SCN], [BMIm][OTf], [BMIm][BF_4], [HMIm][NTf_2], and [OMIm][BF_4]), with a maximum frequency shift of 490 MHz and a detection sensitivity of 185.42 MHz/ε′. In terms of moisture detection, the sensor shows a good resonant response to 0～10% moisture content changes in [EMIm][BF_4] solutions, with a resonant frequency shift of 180 MHz. The metasurface sensor designed in this study has high sensitivity and good measurement repeatability, providing an effective technical means for ionic liquid purity detection and deterioration monitoring, and has important engineering application prospects in fields such as chemical process control and real-time monitoring in hazardous environments.

Key words: Metasurface; Sensor; Ionic liquid; Moisture detection; Trace detection

OCIS Codes: 160.3918; 280.1415; 280.4788

CSTR: 32255.14.gzxb20265503.0355112

Foundation item: National Major Scientific and Technological Projects of Gansu Province (25ZDGE003, 25ZDWA001, 25ZDGE0004, 25ZDGA005), General Project of Joint Research Fund (24JRRA829), Gansu Province Key Research and Development Program-Industrial Project (25YFGA033), Youth Doctoral Fund Project of Gansu Provincial Department of Education (2024QB-036)